

Review

# Wavelet Transform Processor Based Surface Acoustic Wave Devices

Hagar A. Ali <sup>1</sup>, Moataz M. Elsherbini <sup>2,3</sup> and Mohamed I. Ibrahem <sup>2,4,\*</sup>

- <sup>1</sup> Department of Communications and Electronics Engineering, October High Institute for Engineering and Technology, Giza 12573, Egypt
- <sup>2</sup> Department of Electrical Engineering, Faculty of Engineering at Shoubra, Benha University, Cairo 11672, Egypt
- <sup>3</sup> Department of Electrical Engineering, The Egyptian Academy of Engineering and Advanced Technology (EAEAT), El Nahda City 11825, Egypt
- <sup>4</sup> Department of Cyber Security Engineering, George Mason University, Fairfax, VA 22030, USA
- \* Correspondence: mibrahem@gmu.edu

**Abstract:** Due to their numerous advantages, Wavelet transform processor-based acoustic wave devices constitute an interesting approach for various engineering disciplines, such as signal analysis, speech synthesis, image recognition and atmospheric and ocean wave analysis. The major aim of this paper is to review the most recent methods for implementing wavelet transform processor-based surface acoustic wave devices. Accordingly, the goal of this paper is to compare different models, and it will provide a generalized model with small insertion loss values and side lobe attenuation, making it suitable for designing multiplexer filter banks and also to ease the way for the continued evolution of device design. In this paper, a generalized framework on surface acoustic wave devices is presented in terms of mathematical equations, types of materials, crystals types, and interdigital transducer design in addition to addressing some relevant problems.

**Keywords:** WTP; VLSI; SAW; IDT; SER; BAW; IL



**Citation:** Ali, H.A.; Elsherbini, M.M.; Ibrahem, M.I. Wavelet Transform Processor Based Surface Acoustic Wave Devices. *Energies* **2022**, *15*, 8986. <https://doi.org/10.3390/en15238986>

Academic Editor: Maria Grazia De Giorgi

Received: 30 October 2022  
Accepted: 25 November 2022  
Published: 28 November 2022

**Publisher's Note:** MDPI stays neutral with regard to jurisdictional claims in published maps and institutional affiliations.



**Copyright:** © 2022 by the authors. Licensee MDPI, Basel, Switzerland. This article is an open access article distributed under the terms and conditions of the Creative Commons Attribution (CC BY) license (<https://creativecommons.org/licenses/by/4.0/>).

## 1. Introduction

Wavelet technology is considered a robust time-frequency analysis with a strong mathematical base. It represents a relatively new scope of rapid development in applied mathematics and engineering, i.e., instantaneous signals, picture edge identification, image denoising, pattern recognition, data compression, and fractal signal analysis [1–7]. The major motivation for studying the wavelet algorithm for time-frequency dispersive systems is the accurate localization in both time and a frequency domain, which overcomes the problems accompanying Fourier transform analysis. However, its algorithm is convoluted and implemented with difficulty in most fields. To solve this complicated algorithm, many researchers have adopted the concept of implementing wavelet transform processor-(WTP) based hardware devices, such as very large scale integration (VLSI), [8–12] optical devices [13,14] and surface acoustic waves (SAW) [15,16]. In 1993, Parhi et.al [8] proposed two types of VLSI architectures, referred to as the folded architecture and the digit-serial architecture, for the implementation of one-and two-dimensional discrete wavelet transforms. The limitations and positives of the two proposed architectures have been studied and compared. A class of VLSI architectures based on linear systolic arrays for computing the 1-D Discrete Wavelet Transform (DWT) is presented [9] endeavoring to perform better in both computation time and in area. In 1996, Grzeszczak et.al [10] presented an enhanced technique with a new design of that was represented by the authors in [9]. In 2006, Maurizio Martina [11] proposed a new low-complexity, efficient wavelet filter VLSI architecture specified for compressed images. Wavelet has been proposed for biomedical studies [12]; it represents the streaming neurophysiological data based on WTP/VLSI. The

scheme provides efficient bandwidth utilization; conversely, communication costs meant severe limitations on size, energy consumption and power dissipated. Recently, acoustics applications have been commonly used, from noise-removing to ultrasonic imaging. Acoustic-based approaches for biological and biomedical applications have been adopted in the last decade [17,18]. Moreover, the WTP/SAW devices not only can overcome the high power cost for the computer system but also can avoid the big size and low reproducibility for other physics devices, such as optical devices and VLSI [19].

Wavelet transform-based SAW devices present several advantages, as follows [19,20]:

- The complicated conversion of the signal processing is eliminated, which may eliminate the signal distortion;
- Small size;
- Low cost;
- Good temperature stability;
- High reliability and reproducibility;
- Simple implementation techniques of the wavelet transform where the complication of its mathematical algorithms is eliminated.

Based on this strategy, the goals of the paper are listed as follows:

- Provide a unified framework for WTP along with SAW devices by emphasizing their basic elements: the crystal types, design of inter-digital transducers IDT and frequency characteristics;
- Extend the understanding of the existing WTP algorithm by identifying their mathematical relationships with the SAW device interdigital transducers envelop function;
- Simulate the existing SAW devices in the literature concerning their accompanying problem;
- Investigate the trade-offs between different SAW elements;
- Pave the way for further enhancements by providing a wider perspective on WTP using a SAW device;
- Finally, determine the best parameter choices which provide the most side-lobe attenuation and least insertion loss with a neglected effect of a bulk acoustic wave.

The survey is organized as follows: Section 2 presents the wavelet concept and its mathematical representation. The relation between the wavelet function and the envelop function of the SAW interdigital transducer is provided in Section 3.

The dependence of SAW design on mother wavelet specification and their performance are discussed in Section 4. IDT design is then discussed and trade-offs of the SAW elements are investigated in Section 5, accompanying problems and proposed solutions are mentioned in Section 6, and results and simulation are presented in Section 7, while Section 8 concludes the paper.

## 2. Wavelet Analysis

A wavelet is a mathematical tool which breaks data into multiple components and then processes each of them with a convenient scale. There are several time-frequency analysis methods such as Fourier transforms, short-time Fourier transform (STFT) and wavelet analysis, and Ghaderpour et. al, provide a complete study of these techniques with their advantages and limitations including the pre-mentioned ones [21].

Wavelet analysis and Fourier are similar in dealing with the expansion of functions based on basis function sets. However, instead of expanding in terms of trigonometric polynomials, wavelets are generated by scaling and shifts of a function called the mother wavelet. They have a preference for Fourier schemes in physical situations, especially the signal, which contains interruptions and sharp hikes. Fourier transform is a mathematical tool to represent dual dispersive systems; it presents data in frequency but does not show when this frequency has happened. To overcome the limitations of the traditional Fourier transforms, the signal is broken down into smaller components which short-time Fourier transform (STFT) provides [22]. STFT adopted the idea of a fixed time window to represent the signal, by this representation it is safe to say that the signal is stationary over a fixed

interval of time; accordingly, it increases the complexity of implementation given the need to choose an appropriate window size (Figure 1).

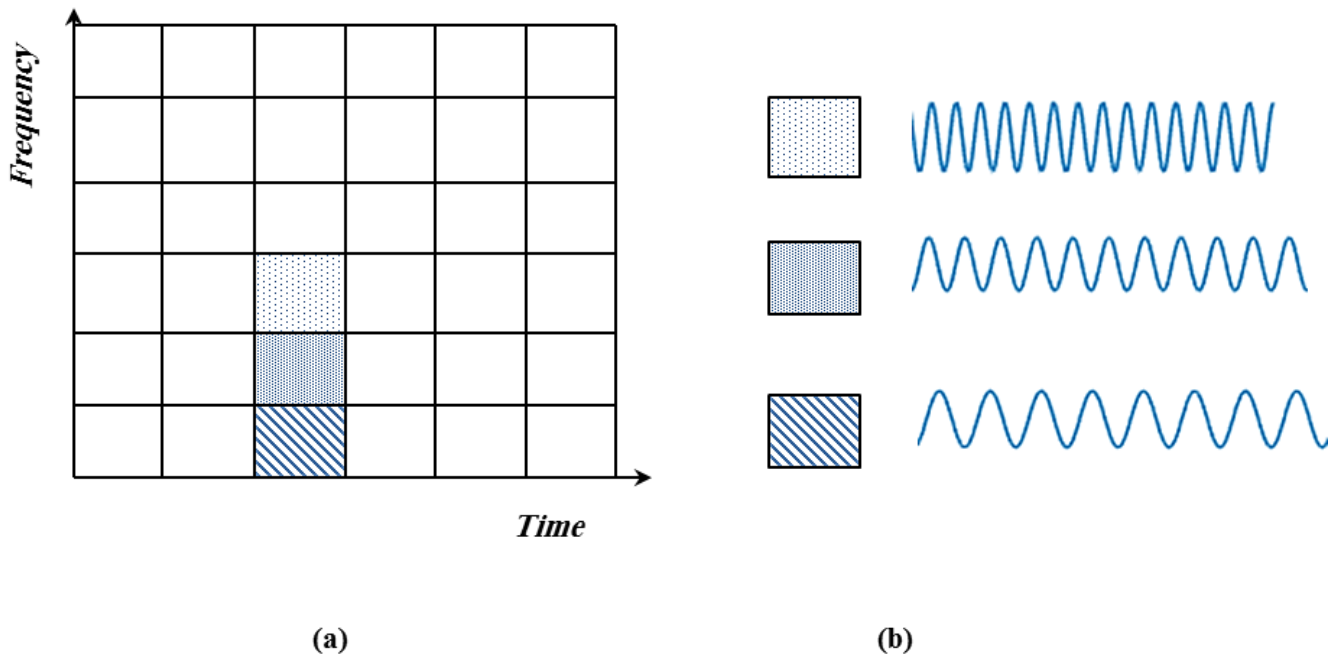


**Figure 1.** Spectrogram of STFT (a) Coverage of Time -Frequency Plane (b) Basis Function.

The STFT presents both the time and the frequency at which a signal occurs. However, determining a window (segment) size is a key problem. For doubly dispersive signal analysis using the STFT, choosing a small window size helps obtain good time resolution but decreases the frequency resolution, and vice versa [23].

Wavelet analysis is capable of adapting a specified function called the mother wavelet. The adaption includes small windows representing high frequency and large windows at low frequency [24]. The original data or function that is represented by the wavelet has been processed by using a linear combination coefficients of those functions [22,23]. One of the features that wavelet presents is the ability to deal with signal discontinuities as depicted from the time-frequency resolution plane [23] (Figure 2).

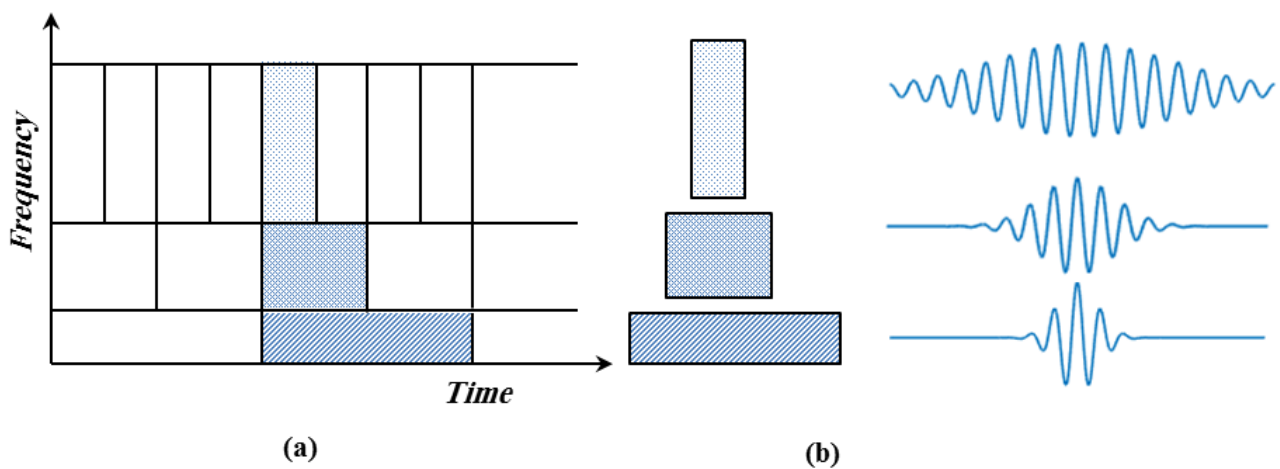


**Figure 2.** Spectrogram of Wavelet Transforms (a) Coverage of Time-Frequency Plane (b) Basis Function.

Figure 2 presents the main idea of wavelet analysis. Once a convenient wavelet function is selected, called a mother wavelet, the analysis is performed by shifted and dilated versions of the mother wavelet. There are scaled (dilated-vertical axis) and trans-

lated (shifted-horizontal axis) versions. Time or space analysis is performed by the high-frequency version of the mother wavelet while the frequency is a dilated low-frequency one. Mathematically, a wavelet can be used to extract information from different data representations such as audio signals and images. Wavelets may decompose the data to be processed with no gaps or overlapping, which is mathematically reversible. Wavelet transforms can be included in the continuous wavelet transform (CWT), the discrete wavelet transform (DWT), and the least-squares wavelet analysis (LSWA). The CWT, DWT and LSWA vary in how they evaluate the scale parameter. The CWT applies exponential scales with radix less than 2. The discrete wavelet transform has dyadic exponential scales. LSWA can process time signals that are irregularly sampled [25,26].

Wavelet transform comprises different wavelet families, each of them including trading-offs between the spatial localization of the basis function (mother wavelet), and its smoothness [27]. Several wavelet names are established according to their inventors (e.g., Daubechies wavelet named for Ingrid Daubechies, Morlet wavelet, Meyer wavelet, and Coiflet wavelets, etc.). The most common types of wavelet basis functions are depicted in Figure 3.

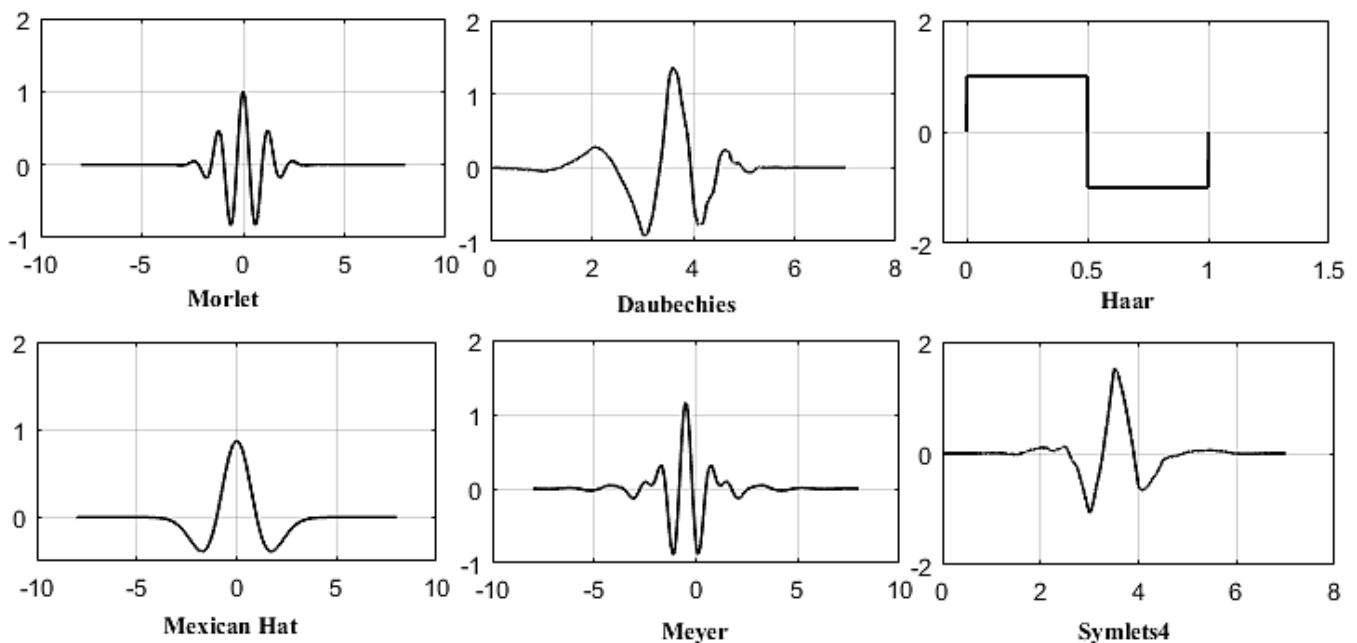


**Figure 3.** Different Mother Wavelet Functions.

The wavelet basis is defined as [23,28,29]

$$\psi_{s,l}(t) = \frac{1}{\sqrt{s}} \psi\left(\frac{t-l}{s}\right) \quad (1)$$

where  $\psi(t)$  is the mother wavelet function,  $s$  and  $l$  are the scale and shift factors respectively. The scaled index indicates the wavelet width and  $l$  gives the position. The wavelet transform can break down a signal into various decaying resolution levels by adjusting the scale and shift factors of a wavelet function, therefore, once knowing the mother wavelet, everything about the basis has been known. In this paper, we will focus on continuous wavelet transform-based Morlet wavelet (Figure 4). The advantage of using a Morlet wavelet is that it provides an optimal time-frequency resolution spectrogram [21,25], and it will be presented in detail in the next section.

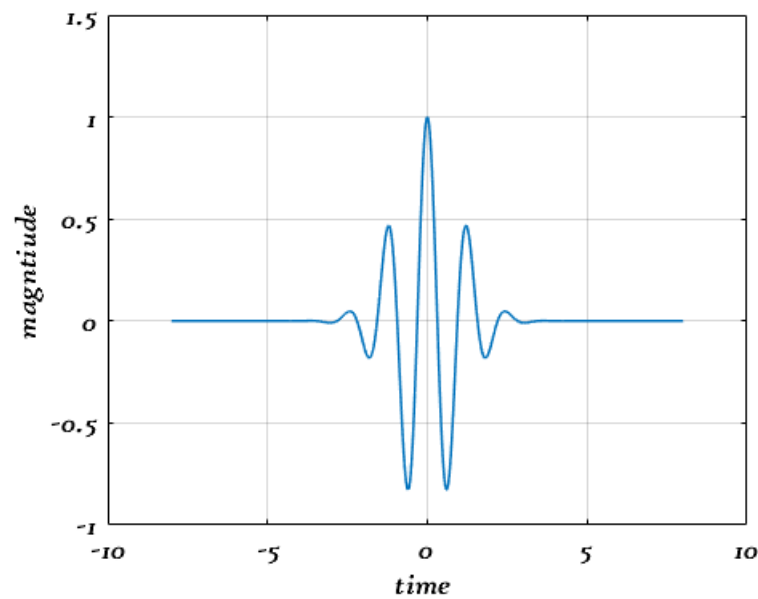


Figure 4. Real-Valued Morlet Wavelet Function.

### 3. SAW Design-Based Morlet Wavelet Function

Implementing WTP/SAW devices is based on designing the input interdigital transducer overlap to be a morlet function envelope. Therefore, the input IDTs is morlet-based while, the output IDTs is uniform. Figure 5 represents the difference between a uniform design and a morlet-based envelope. The impulse response is given by Equation (2) [20].

$$h(t) = Ae^{j\omega_0 t} \quad (2)$$

where  $A$  is a constant.

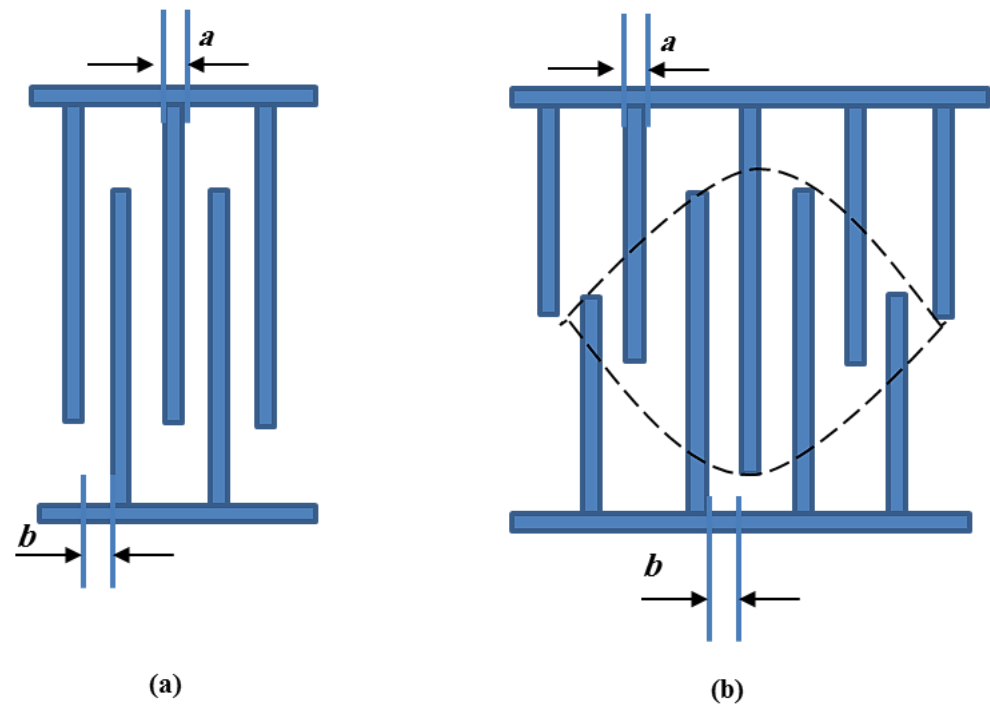


Figure 5. (a) IDT with equal finger overlap (uniform) (b) IDT with Morlet wavelet.

The Morlet wavelet is mathematically represented by the multiplication of complex exponential and Gaussian windows as follows [30–32].

$$\psi(t) = \frac{1}{\sqrt{s}} e^{-\frac{1}{2}(\frac{t}{s})^2} e^{j\omega_0 t} \quad (3)$$

Comparing Equations (2) and (3), conclusively if  $A$  is a function of time  $A(t) = \frac{1}{\sqrt{s}} e^{-\frac{1}{2}(\frac{t}{s})^2}$  it will establish a wavelet type of transmitting IDT impulse response. The difference between uniform finger overlap and wavelet-based finger overlap is depicted in Figure 5.

#### 4. The Performance of WTP-Based SAW Device

To implement a wavelet transform processor-based SAW device, two specially designed interdigital transducers (IDTs) were fabricated on a substrate. The selection of the substrate material controls the performance of the SAW device. There are some parameters like propagation speed, the electromechanical coupling coefficient (ECC), temperature coefficient and propagation loss, which depend on the substrate material as depicted in Table 1 [33].

Concerning Table 1, the two most important practical material parameters employed in SAW device design are the electromechanical coupling coefficient ( $K^2$ ) and the SAW velocity. ECC is a measure of the competence of a material in turning an input electrical signal into mechanical counterpart energy; the values are too small, so they are expressed in percentages [33].

**Table 1.** SAW parameters of selected substrate materials [33].

Material	Crystal Cut	SAW Axis	Velocity (m/s)	$K^2$ (%)	Temperature Coefficient of Delay (ppm/°C)
Quartz	ST	X	3158	0.11	0
LiNbO <sub>3</sub>	Y	Z	3488	4.5	+94
LiNbO <sub>3</sub>	128°	X	3992	5.3	+75
Bi <sub>12</sub> GeO <sub>20</sub>	110	001	1681	1.4	+120
LiTaO <sub>3</sub>	Y	Z	3230	0.72	+35
GaAs	<001>	(110)	<2841	<0.06	−49

However, the values of velocity depicted in the previous table are also affected by the physical properties of the selected material (i.e., elasticity, density and piezoelectric properties), these parameters can all change with temperature. Also, temperature changes will cause phase shifts that may reduce the stability of the SAW device. In addition to the materials in the previous table, high-temperature SAW devices, such as piezoelectric materials and metal electrodes, are proposed and studied [34,35], the studies analyze the stability and lifetime of SAW devices in harsh environments. Several types of substrate materials are examined such as platinum (Pt), lead zirconate titanate (PZT), calcium copper titanate (CCTO), and carbon nanotubes (CNTs).

Generally, SAW substrate materials are anisotropic. This gives different propagation characteristics with different crystal cut directions. It requires the use of a substrate with appropriate crystal cuts for the avoidance of any performance degradation, and the orientation cut of the lattice diagram related to material fabrication represented in the second and third columns is the best for the selected materials.

YZ lithium niobate (LiNbO<sub>3</sub>) is generally applied in wideband filters due to the high-velocity values which introduce a small size in practical implementation. 128-rotated X propagating lithium niobate is a special cut designed for reduced bulk wave generation over its Y-Z counterpart; the bulk acoustic wave effect will be discussed in Section 6.1.

ST-X quartz (i.e., stable temperature cut), appeared efficiently in narrow-band filters with high stability (zero temperature coefficient). Lithium tantalate has a higher ECC than

ST-X quartz and conversely poorer temperature stability. Of the remaining SAW substrates depicted in Table 1, bismuth germanium oxide ( $\text{Bi}_{12}\text{GeO}_{20}$ ) has found use in long-delay line applications with low SAW velocity. The piezoelectric coupling of gallium arsenide (GaAs) is slightly less than quartz, while its detraction is high.

In this section, the effect of some parameters related to substrate selection will be discussed. The foremost ECC of the substrate material affects the relative bandwidth and insertion loss (IL), so the appropriate relationship between them helps in the selection of substrate material.

#### 4.1. ECC Value as a Function of Centre Frequency and Wavelet Scale

As mentioned earlier, to implement a wavelet transform processor-based SAW device, two specially designed IDTs are required: the input IDT design-based Morlet wavelet envelope and output uniform IDT. Accordingly, the mathematical relationship between them will be analyzed.

The frequency domain of Equation (2) is denoted by the following expression [36]:

$$\psi(\omega) = \frac{\sqrt{\pi}}{\sqrt{s}} e^{-\frac{1}{2}s^2(\omega-\omega_0)^2} \quad (4)$$

where  $\omega_0$  is the central angle frequency function.

$$Y(\omega) = \frac{\psi(\omega)}{\frac{\sqrt{\pi}}{\sqrt{s}}} = e^{-\frac{1}{2}s^2(\omega-\omega_0)^2} \quad (5)$$

$$Y(\omega) = 10^{-\frac{3}{20}}$$

then,

$$\Delta f_{-3\text{dB}} = \frac{1}{2\pi s} \sqrt{-2 \ln(10^{-\frac{3}{20}})} = \frac{0.1323}{s} \quad (6)$$

The output IDT is uniform and its bandwidth is much bigger than the input, so the Morlet wavelet transform processor depends on the input, meanwhile, the maximum fractional bandwidth for output IDT (unapodized) [33] is

$$\frac{\Delta F_{-3\text{dB}}}{f_0} = 2\sqrt{\frac{K^2}{\pi}} = 1.1283\sqrt{K^2} \quad (7)$$

where  $K^2$  is the ECC of the substrate material. Accordingly, from Equations (6) and (7) so there must be  $\Delta F_{-3\text{dB}} \geq \Delta f_{-3\text{dB}}$  [19], ECC values may be

$$K^2 \geq \frac{0.01375}{f_0^2 s^2} \quad (8)$$

#### 4.2. The Influence of ECC on IL

The mathematical expression of the insertion loss of the SAW device is represented by Equation (9) [33]. The equation provides the value of insertion loss can be held to 6 db before external circuit responses prevail at maximum bandwidth

$$IL = 10 \log_{10} \left( \frac{\pi}{2K^2} \right)^2 \left( \frac{\Delta f}{f_0} \right)^4 \quad (9)$$

where  $K^2$  is the electromechanical coupling coefficient,  $f_0$  is the center frequency.

The frequency response is limited to the input IDT, the frequency of the output is much bigger than the input, as it is a uniform IDT. Substituting  $(\frac{\Delta f}{f_0})$  Equation (6) given

$$IL = -31.215 - 20 \log_{10} K^2 - 10 \log s^4 f_0^4 \quad (10)$$

According to Equation (10), choosing a material with large  $K^2$  will reduce IL, it will be a trade-off with the design we will introduce later.

### 5. Interdigital Transducer Design

Implementing a wavelet processor-based SAW device requires the input IDT geometry designed as a Morlet wavelet envelope and the output IDT to be uniformly designed [19,36] (Figure 6).

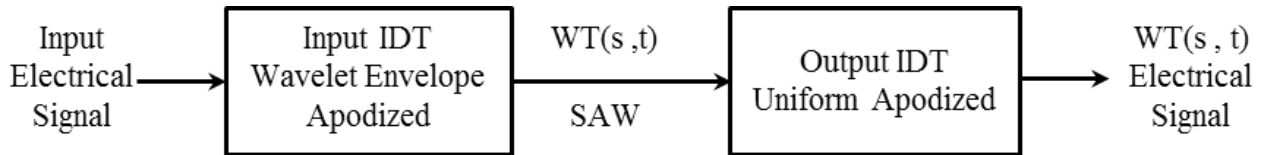


Figure 6. Principle of Single Scale Wavelet Transforms.

#### 5.1. Specifications of the Input IDT Design

According to the wavelet principals and with Nyquist sampling theory, the sampling time of each interdigital electrode is

$$\Delta t = \frac{1}{2f_0} \tag{11}$$

Then the sampling time of all interdigital electrodes is [19]

$$t(n) = \frac{n - 1}{2f_0} \tag{12}$$

where  $n$ : is the numbering sequence of the interdigital electrode pairs. The wavelet envelope represented by Equation (3) can be used to determine the overlapping length of interdigital transducer fingers by the following formula [19,37].

$$L(n) = L_{max} e^{-\frac{(n-1)^2}{8s^2 f_0^2}} \tag{13}$$

So

$$n = \sqrt{8s^2 f_0^2 \ln \frac{L_{max}}{L(n)}} + 1 \tag{14}$$

Let  $L(n) = L_{min}$  then input IDT number ( $N$ ) can be deduced from the formula

$$N = \sqrt{8s^2 f_0^2 \ln \frac{L_{max}}{L_{min}}} + 1 \tag{15}$$

From the previous equations, once center frequency and wavelet scale are selected, we can get the number of IDT fingers and their overlapped lengths.

#### 5.2. Specifications of the Output IDT Design

Mathematical relations applied to SAW design by equivalent circuit models are mentioned in this section. According to the Mason model, the output IDT is represented by the electrical circuit of the parallel combination of capacitance, conductance and susceptance Figure 7 [38].

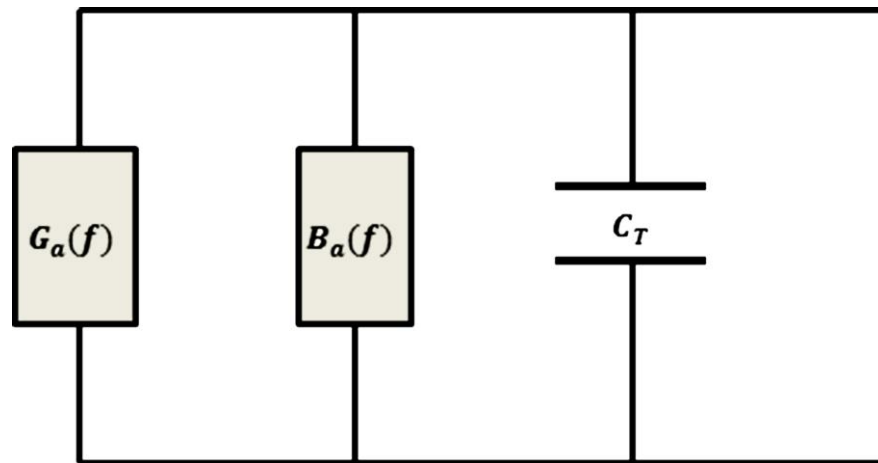


Figure 7. Equivalent circuit Model for Output IDT.

Where  $G_a(f)$ ,  $B_a(f)$  is the radiation conductance and radiation susceptance, respectively, and the radiation conductance near the center frequency is deduced from the equation [19,33].

$$G_a(f) = G_a(f_0) \left( \frac{\sin(M\pi((f - f_0)/f_0))}{M\pi((f - f_0)/f_0)} \right)^2 \tag{16}$$

$M$  is the number of output IDT.

The zero crossings of the sinc function occurred when  $M\pi((f - f_0)/f_0) = \pm\pi$ , the 3 dB bandwidth is evaluated as the halved frequency period from frequency  $f$  to the center frequency given by Equation (17) [19].

$$\Delta f_{-3dB} = \frac{f_0}{M} \tag{17}$$

As mentioned before, the bandwidth is limited to the input IDT, applying the Gabor uncertainty condition for a doubly dispersive channel, so Equation (17) will be as follows [30].

$$\Delta f_{-3dB} = \frac{0.883f_0}{M} \tag{18}$$

The finger number can be calculated as the value at which the 3 dB value of the input IDT must be lower than the value of the output IDT. It will be given by

$$\frac{0.883f_0}{M} \geq \frac{0.1323}{s} \tag{19}$$

$$M \leq \lfloor 6.6742f_0s \rfloor \tag{20}$$

where  $\lfloor \blacksquare \rfloor$  provides a maximum integer less than a given number.

## 6. Accompanying Problems

Some problems adversely dominated the performance of wavelet processor-based SAW; accordingly, these problems have led to some design trade-offs. We will discuss them briefly, as well as some of the proposed solutions to reduce their impact.

The three key problems of wavelet transform processor-based SAW devices [36] are defined as the bulk acoustic wave (BAW), the sound-electricity reclamation (SER), and the insertion loss. The following sub-sections will discuss their effects.

### 6.1. The Bulk Acoustic Wave

The excitation of IDT on the piezoelectric surface generates bulk acoustic waves in addition to the launching of surface waves. The generation of BAWs affects to the amount

of power that is consumed from the total power. Thus, the ratio of the BAW power to the total power must be decreased. The greater the number of finger pairs the smaller the amount of BAW generation (Table 2) [19,33,39].

**Table 2.** SAW Power and BAW Power Related to Total Power [19,39].

Finger Pair M	The Ratio of SAW Power to Total Power%	The Ratio of BAW Power to Total Power%
1	42.8	52.7
5	87.7	12.3
20	98.3	1.7

There is another problem due to the BAWs generation. BAWs decrease the performance of the SAW filter, causing passband ripples, the distortion of phase and amplitude, and an increase in the insertion loss [40] Figure 8.

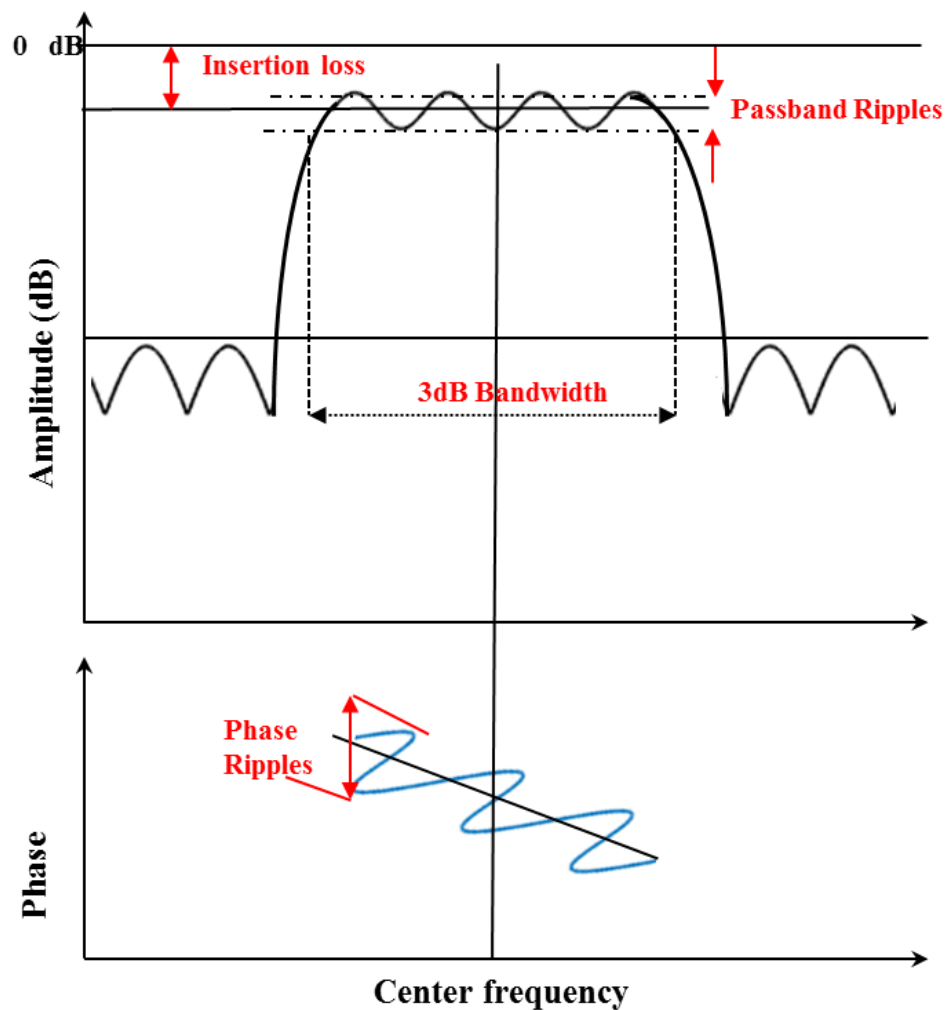


**Figure 8.** Schematic frequency and phase response of a SAW band-pass filter.

From Table 2, the effect of BAWs can be omitted, as M is larger than 20. The number of IDT fingers can be selected value in  $(20, [6.6742f_0s])$ .

6.2. The Sound Electricity Reclamation

The sound electricity reclamation delays or stores some input energy, thus a reflection of the incident sound wave for IDT occurs and led to performance detraction. The SER is related to the electromechanical coupling coefficient  $K^2$ , where the larger ECC is the stronger SER effect [39].

### 6.3. The Insertion Loss

Equation (10) theoretically presents the factors that affected  $IL$  value predominantly, and the electromechanical coupling coefficient value controls the performance of the SAW devices. It is better to choose the material with a large ECC to reduce the  $IL$  value. The ECC is commensurate to the relative change in velocity Equation (21) [33]

$$K^2 = 2 \left| \frac{\Delta v}{v} \right| \quad (21)$$

The relative change of velocity  $\left| \frac{\Delta v}{v} \right|$  arises from the SAW propagation across metal finger from free crystal which causes shorting out of the tangential electric field and the velocity to be decreased.

As a result of impedance change at the edges of IDTs, the reflection of SAWs occurs. That reflection causes fluctuations in appearance in the passband and asymmetrical frequency response. The intensity of the reflected SAW is related to the impedance ratio  $\frac{Z}{Z_0}$  [41].

The change of the impedance caused by the metal film is given by [33]

$$\frac{Z}{Z_0} = \left| \frac{\Delta v}{v} \right| = \frac{K^2}{2} \quad (22)$$

It is more convenient to choose a substrate material with a small ECC to reduce the asymmetry of frequency response.

There are several factors that affect the performance of WTP/SAW devices. These factors are the electromechanical coupling coefficient, the maximum relative bandwidth, insertion loss, the sound electricity reclamation and the reflection generated by IDT. Decreasing the insertion loss requires ECC to be as large as possible as depicted by Equation (7); on the other hand, the reflection generated by IDT and SER requires the ECC as small as possible, it is necessary to make a trade-off.

### 6.4. The Selection of the Substrate Material

Many parameters determine the substrate materials such as propagation velocity  $v_s$ , the electromechanical coupling coefficient  $K^2$ , the temperature coefficient, and propagation loss. However, the critical key parameters are propagation velocity and ECC, thus choosing material requires a trade-off between them. The effect of ECC has been mentioned, and now the effect of the propagation velocity will be discussed.

The dimensions of the IDT fingers are the width ( $a$ ) and ( $b$ ) is the interval between fingers. The lengths are related to  $\lambda$ , with a metallization ratio of 50% [20].

$$\lambda = 2a + 2b \quad (23)$$

$$a = b = \frac{v_s}{4f_0} \quad (24)$$

### 6.5. The Diffraction Problem from Input IDT to Output IDT

Gao et al. [42], presented the diffraction problem occurs with SAW propagation from input to output by the diffraction equation of classical optics as [33]

$$F = \frac{\lambda D}{A^2} \quad (25)$$

$A$  is the aperture width,  $D$  is the distance from the input IDT to the output IDT and  $F$  is the dimensionless (Fresnel) parameter which may be less than 1 or greater than 1 corresponding to the Fresnel (near-field) or Fraunhofer (far-field) regions respectively as depicted by Figure 9 [42].

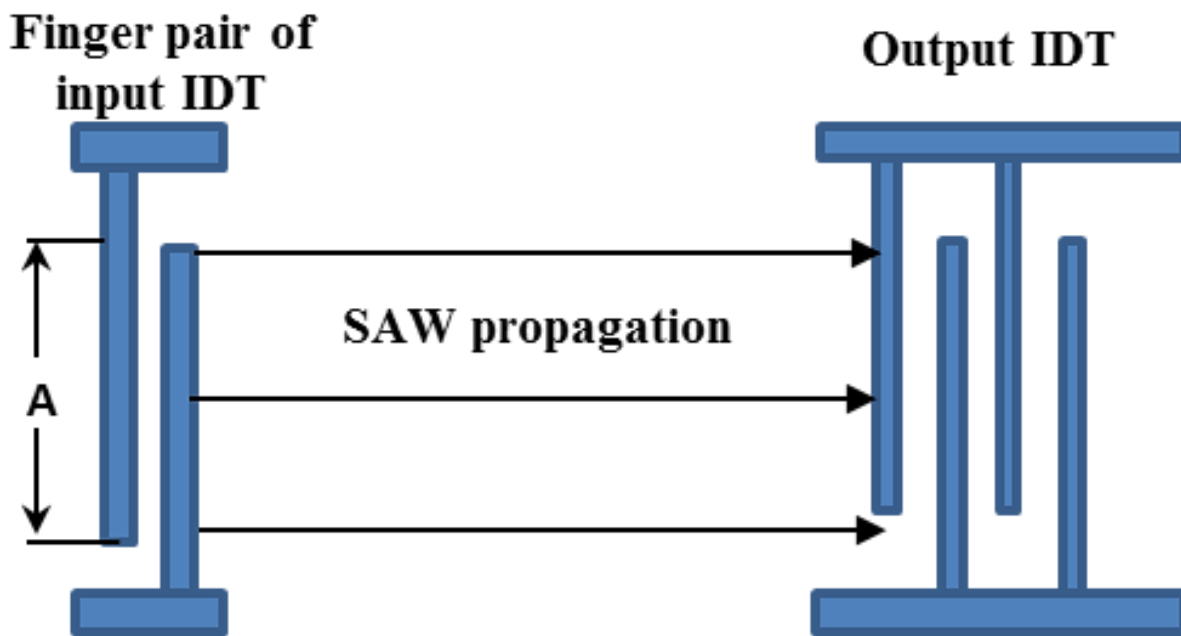
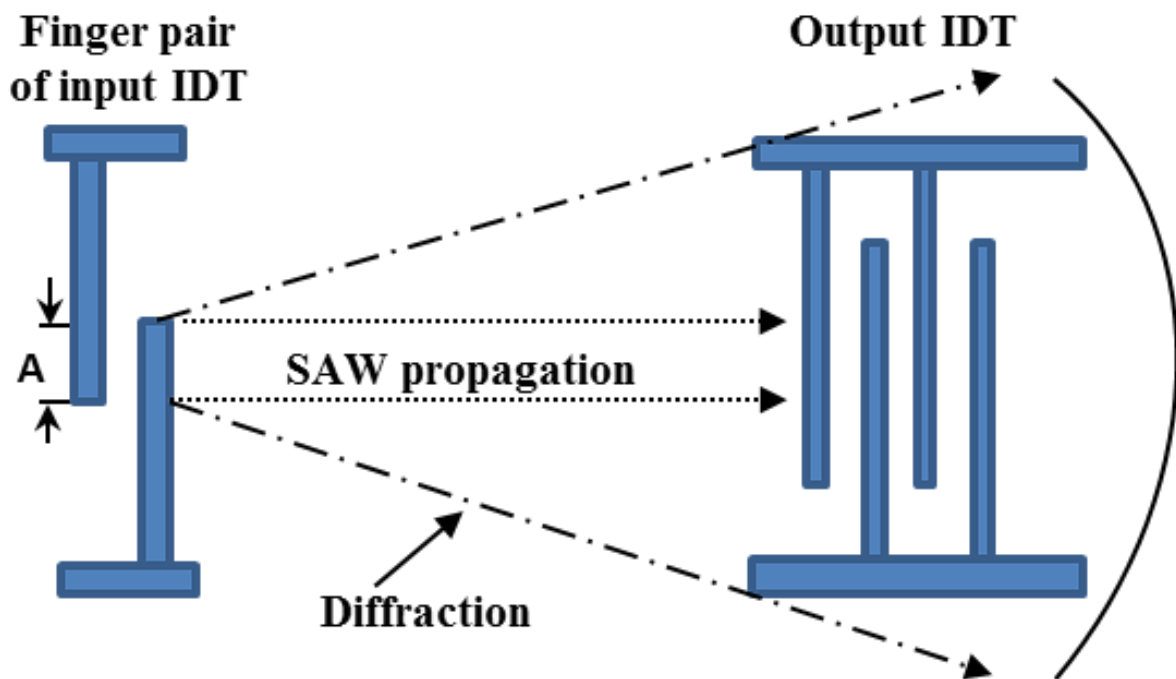


**Figure 9.** Input/output IDTs (a) far-field (b) near-field.

To conserve the SAW beams as parallel beams, the distance from input IDT to output one is based on the near field region so  $F < 1$  gives

$$D < \frac{A^2}{\lambda} \tag{26}$$

If the interval between the two IDT is  $L_g$  which preserves the near-field basis, then the total length of the WTP is given by [19]

$$L = 2Na + 2Ma + L_g - 2a \tag{27}$$

The choice of the substrate may require a material with high propagation velocity  $v_s$  to increase the finger width (Equation (14)). Increasing the finger width and the interval between the fingers accordingly decreases the difficulty of production, but it will be a trade-off with the total package size Equations (14) and (17).

## 7. Results

To verify the equations listed later, a comparison among three related papers will be established, and the results of those works will be presented and compared. The section also includes verification that was established using the suitable simulation tool of selected works for proposing a novel design for our future work. The input IDTs are uniformly spacing Morlet apodized. As the output IDT is unapodized, accordingly, the impulse model can be applied [43–50]. Table 3 presents the simulation parameters used in the works being compared.

**Table 3.** Simulation Parameters.

Reference	Substrate Material	$K^2$	SAW Velocity (m/s)	Processing Time ( $\mu$ s)	Scale	Max Aperture Length ( $\mu$ m)	Center Frequency (MHz)	Theoretical $-3$ dB Bandwidth (MHz)	Number of Electrode Pairs	
									Input	Output
[39]	X $112^\circ$ Y LiTaO <sub>3</sub>	0.75	3295	1.7	2–1	2000	34.323	0.2645	100	24
					2–2		68.646	0.52911		
					2–3		137.292	1.0582		
[39]	Y-Z LiNbO <sub>3</sub>	4.5	3488	1.47	2–1	2000	68.646	0.52911	100	24
[19]	X $112^\circ$ Y LiTaO <sub>3</sub>	0.75	3295	1.7	0.3149	2200	61.6	0.42006	106	21
[51]	ST-X quartz	0.11	3158	1.89	0.2152	3433.5	60	0.6148	117	49

The previous table represents the parameters the works [19,36,48] have used. The practical results provided us with information about the effect of choosing the number of IDT at input and output, the material selected (i.e., ECC, velocity, and processing time), wavelet scale (controls the center frequency and bandwidth) on the insertion loss and side-lobe attenuation to get the most efficient performance.

Lu et al. [39] measured the bandwidth and insertion loss for different wavelet scales using the network analyzer HP8712ET. The practical results provide decreasing insertion loss with increasing frequency. In 2017, Wenke Lu proposed new design parameters with the same substrate material to reduce some of the defects related to his previous design [19], and experimental results were measured by an E5061A network analyzer. The result presents more stability in passband ripples and side-lobe attenuation.

In 2022, Lu et al. applied the technique of unbalanced split electrode IDTs to compensate the BAW, reduce passband ripples and attenuate the side-lobes [51]. The experimental results were measured by an E5061A network analyzer.

The figures below show the simulated frequency characteristic curves of the equivalent circuit of Figure 7. The results were measured by a simulation tool that represents a wavelet processor SAW device [19,39,51].

Figures 10–12 represent the frequency response characteristic of different substrate materials with different parameters selected. There is a small insertion loss with the accepted 3dB bandwidth as depicted in Figure 10, thus conversely side-lobe attenuation is better with ST-quartz, as in Figure 12. Table 4 represents different simulated values of insertion loss and side-lobe attenuation of three selected works.

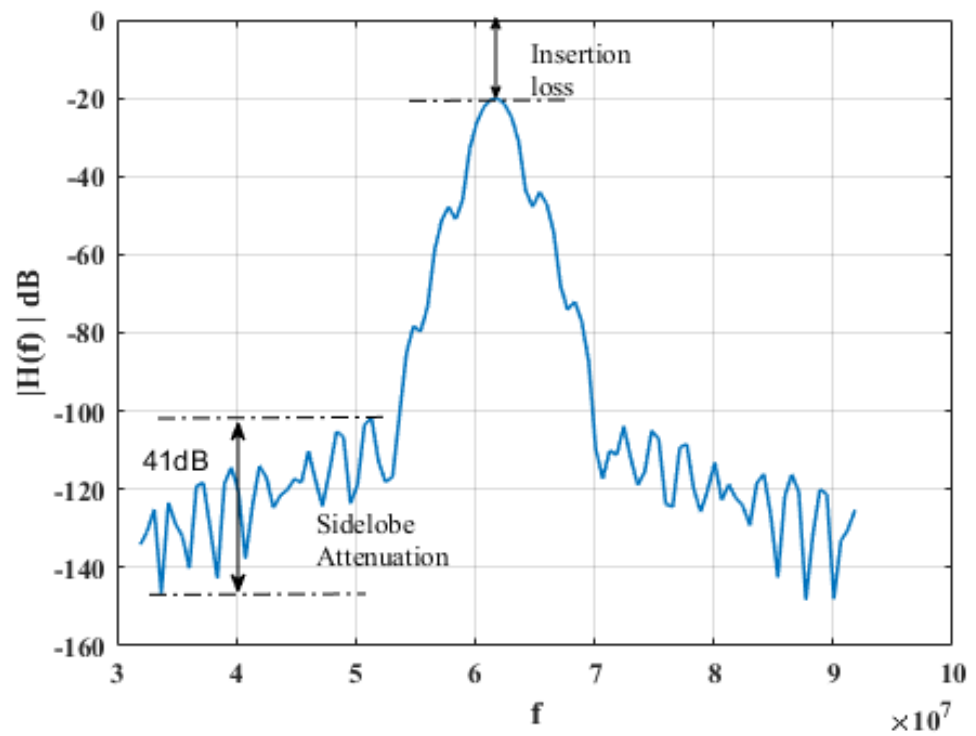


Figure 10. The Frequency Response characteristic X 112° Y LiTaO<sub>3</sub>.

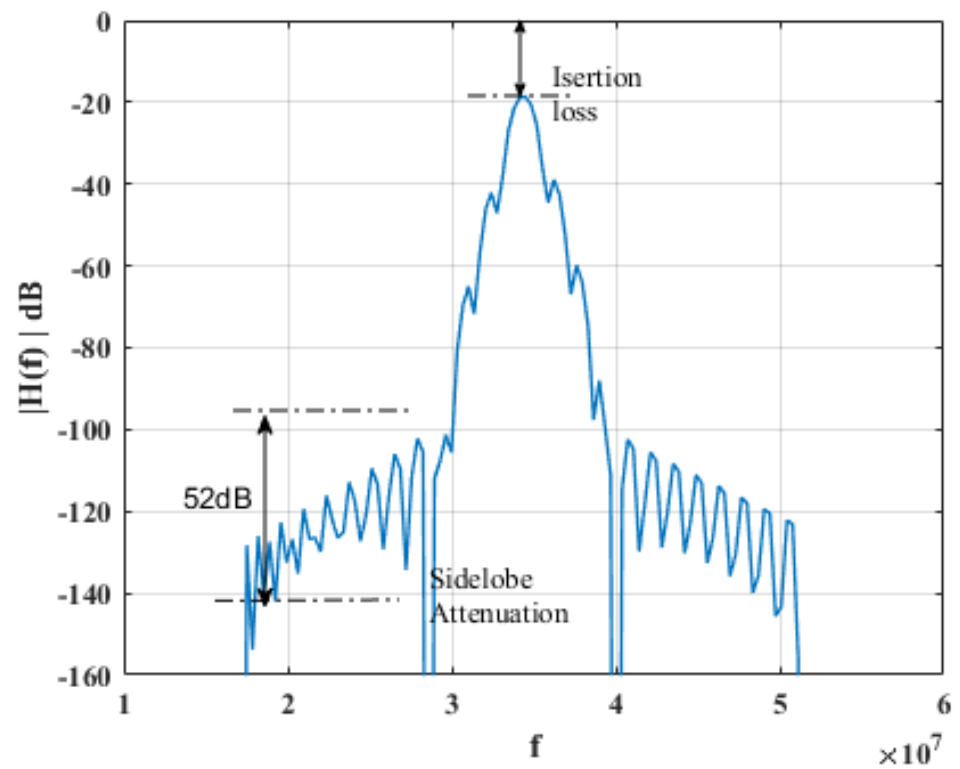


Figure 11. The Frequency Response characteristic Y-Z LiNbO<sub>3</sub>.

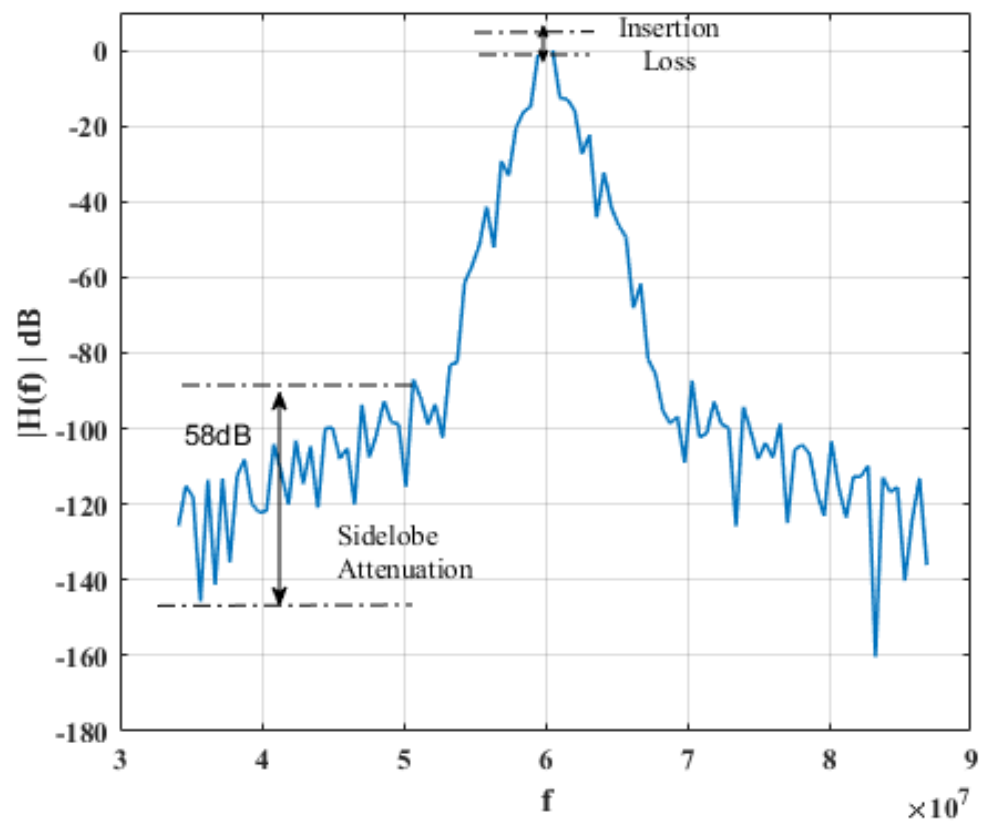


Figure 12. The Frequency Response characteristic ST-X Quartz.

Table 4. Simulated Results For Insertion Loss and Sidelobe Attenuation.

References	[39]	[19]	[51]
Insertion loss	-19	-20	-6
Sidelobe attenuation (dB)	41	52	58

The advantages and disadvantages of wavelet transform processor-based SAW devices are listed in Table 5.

Table 5. The Advantages and Disadvantages of WTP-based SAW Devices.

Advantages	Disadvantages
Complicated conversion of the signal processed is eliminated, which may eliminate the signal distortion.	Limitation on bandwidth values.
Small size.	Limitation on the number of input/output IDTs fingers.
Low cost.	The center frequency and wavelet scale are dependent variables which pose a challenge in parameter selection.
Good temperature stability.	The sound electricity reclamation and insertion loss are two trade-offs related to ECC.
High reliability and reproducibility.	The symmetry of frequency response is another challenge in choosing substrate material, as it depends on the ECC value.

### 8. Conclusions

Wavelet transform is considered robust time-frequency analysis that provides accurate localization in both time and frequency domains. Studying the wavelet algorithm for time-frequency dispersive systems provides sufficient localization in both domains. In this survey, the design of surface acoustic wave devices is a simple powerful method for the wavelet transform processors. Wavelet processor-based SAW devices with a single

scale are passband filters. The major motivation of this work is to compare different substrate materials and design parameters which perform the WTP-SAW devices efficiently as passband filters for our future work.

The survey is examined based on the concept of solving the main problems that appear in the design. The framework categorizes the SAW device schemes based on their substrate materials, electromechanical coupling coefficient, and bulk acoustic wave. The survey presents a framework to apply and study new schemes of signal processing techniques, which may pave the way for further developments of WTP-SAW based. Finally, the motivation of this paper was to implement a generalized model that presented a WTP-based SAW device with small insertion loss values and sidelobe attenuation, making it suitable for designing multiplexer filter banks. Accordingly, a comparison of previous studies has been adopted. The comparison includes several substrate materials, different values of center frequency and scales.

Figure 13 describes the statistics of the papers related to our work; therefore it provides information about the number of publications and the year of publication.

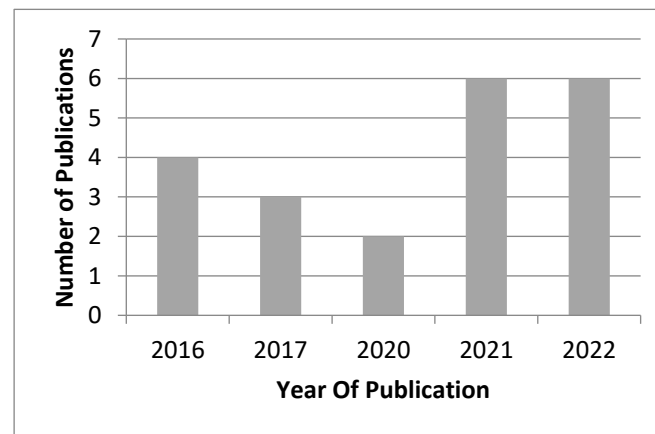


Figure 13. Related Works.

**Author Contributions:** Conceptualization, H.A.A., M.M.E. and M.I.I.; methodology H.A.A., M.M.E. and M.I.I.; investigation, H.A.A., M.M.E. and M.I.I.; writing—original draft preparation, H.A.A.; writing—review and editing, M.M.E.; supervision, M.I.I.; resources, H.A.A., M.M.E. and M.I.I.; data curation, H.A.A., M.M.E. and M.I.I.; visualization, M.M.E. and M.I.I. All authors have read and agreed to the published version of the manuscript.

**Funding:** This research received no external funding.

**Data Availability Statement:** Not applicable.

**Conflicts of Interest:** The authors declare no conflict of interest.

### Abbreviations

WTP	Wavelet transform processor
VLSI	Very-large-scale integration
SAW	Surface acoustic wave
IDT	Interdigital transducer
CWT	Continues wavelet transform
DWT	Discrete wavelet transform
LSWA	Least-squares wavelet analysis
STFT	Short time Fourier transform
SER	The sound electricity reclamation
BAW	Bulk acoustic wave
IL	Insertion loss
ECC	Electromechanical coupling coefficient

## References

1. Shi, B.; Cao, M.; Wang, Z.; Ostachowicz, W. A directional continuous wavelet transform of mode shape for line-type damage detection in plate-type structures. *Mech. Syst. Signal Process* **2022**, *167*, 108510. [[CrossRef](#)]
2. Li, C.; Yu, Y.; Yang, Z.; Liu, Q.; Peng, X. ESR estimation for aluminum electrolytic capacitor of power electronic converter based on compressed sensing and wavelet transform. *IEEE Trans. Ind. Electron.* **2021**, *69*, 1948–1957. [[CrossRef](#)]
3. Hong, H.P.; Cui, X.Z.; Qiao, D. Simulating nonstationary non-Gaussian vector process based on continuous wavelet transform. *Mech. Syst. Signal Process* **2022**, *165*, 108340. [[CrossRef](#)]
4. Psaras, V.; Tzelepis, D.; Vozikis, D.; Adam, G.P.; Burt, G. Non-unit protection for HVDC grids: An analytical approach for wavelet transform-based schemes. *IEEE Trans. Power Deliv.* **2020**, *36*, 2634–2645. [[CrossRef](#)]
5. Bilgili, F.; Lorente, D.B.; Kuşkaya, S.; Ünlü, F.; Gençoğlu, P.; Rosha, P. The role of hydropower energy in the level of CO2 emissions: An application of continuous wavelet transform. *Renew. Energy* **2021**, *178*, 283–294. [[CrossRef](#)]
6. Li, X.X.; Li, D.; Ren, W.X.; Zhang, J.S. Loosening Identification of Multi-Bolt Connections Based on Wavelet Transform and ResNet-50 Convolutional Neural Network. *Sensors* **2022**, *22*, 6825. [[CrossRef](#)]
7. Mahmood, M.R.; Matin, M.A.; Sarigiannidis, P.; Goudos, S.K. A Comprehensive Review on Artificial Intelligence/Machine Learning Algorithms for Empowering the Future IoT Toward 6G Era. *IEEE Access* **2022**, *10*, 87535–87562. [[CrossRef](#)]
8. Parhi, K.K.; Nishitani, T. VLSI architectures for discrete wavelet transforms. *IEEE Trans. Very Large Scale Integr. Syst.* **1993**, *1*, 191–202. [[CrossRef](#)]
9. Vishwanath, M.; Owens, R.M.; Irwin, M.J. VLSI architectures for the discrete wavelet transform. *IEEE Trans. Circuits Syst. II Analog. Digit. Signal Process* **1995**, *42*, 305–316. [[CrossRef](#)]
10. Grzeszczak, A.; Mandal, M.K.; Panchanathan, S. VLSI implementation of discrete wavelet transform. *IEEE Trans. Very Large Scale Integr. Syst.* **1996**, *4*, 421–433. [[CrossRef](#)]
11. Martina, M.; Maserà, G. Low-complexity, efficient 9/7 wavelet filters VLSI implementation. *IEEE Trans. Circuits Syst. II Express Briefs* **2006**, *53*, 1289–1293. [[CrossRef](#)]
12. Oweiss, K.G.; Mason, A.; Suhail, Y.; Kamboh, A.M.; Thomson, K.E. A scalable wavelet transform VLSI architecture for real-time signal processing in high-density intra-cortical implants. *IEEE Trans. Circuits Syst. I Regul. Pap.* **2007**, *54*, 1266–1278. [[CrossRef](#)]
13. Wong, A.C.; Peng, G.D. Applications of Discrete Wavelet Transform in Optical Fibre Sensing. In *Discrete Wavelet Transforms—Biomedical Application*; IntechOpen: London, UK, 2011; pp. 221–248. [[CrossRef](#)]
14. Cincotti, G.; Moreolo, M.S.; Neri, A. Optical wavelet signals processing and multiplexing. *EURASIP J. Adv. Signal Process* **2005**, *2005*, 742803. [[CrossRef](#)]
15. Wen, C.; Zhu, C. Time synchronous dyadic wavelet processor array using surface acoustic wave devices. *Smart Mater. Struct.* **2006**, *15*, 939. [[CrossRef](#)]
16. Lu, W.; Zhu, C.; Liu, Q.; Zhang, J. Implementing wavelet inverse-transform processor with surface acoustic wave device. *Ultrasonics* **2013**, *53*, 447–454. [[CrossRef](#)] [[PubMed](#)]
17. Mazalan, M.B.; Noor, A.M.; Wahab, Y.; Yahud, S.; Zaman, W.S.W.K. Current Development in Interdigital Transducer (IDT) Surface Acoustic Wave Devices for Live Cell In Vitro Studies: A Review. *Micromachines* **2021**, *13*, 30. [[CrossRef](#)]
18. Samarentsis, A.G.; Pantazis, A.K.; Tsortos, A.; Friedt, J.M.; Gizeli, E. Hybrid sensor device for simultaneous surface plasmon resonance and surface acoustic wave measurements. *Sensors* **2020**, *20*, 6177. [[CrossRef](#)]
19. Liu, S.; Lu, W.; Feng, Y. Research on three key problems of the design of the wavelet transform processor using surface acoustic wave devices. *IET Circuits Devices Syst.* **2017**, *11*, 1–6.
20. Lu, W.; Zhu, C.; Liu, J.; Liu, Q. Implementing wavelet transform with SAW elements. *Sci. China Ser. E Technol. Sci.* **2003**, *46*, 627–638. [[CrossRef](#)]
21. Ghaderpour, E.; Pagiatakis, S.D.; Hassan, Q.K. A survey on change detection and time series analysis with applications. *Appl. Sci.* **2021**, *11*, 6141. [[CrossRef](#)]
22. Galli, A.W.; Heydt, G.T.; Ribeiro, P.F. Exploring the power of wavelet analysis. *IEEE Comput. Appl. Power* **1996**, *9*, 37–41. [[CrossRef](#)]
23. Graps, A. An introduction to wavelets. *IEEE Comput. Sci. Eng.* **1995**, *2*, 50–61. [[CrossRef](#)]
24. Vetterli, M.; Herley, C. Wavelets and filter banks: Theory and design. *IEEE Trans. Signal Process* **1992**, *40*, 2207–2232. [[CrossRef](#)]
25. Ghaderpour, E. Least-squares wavelet and cross-wavelet analyses of VLBI baseline length and temperature time series: Fortaleza–Hartebeesthoek–Westford–Wetzell. *Publ. Astron. Soc. Pac.* **2021**, *133*, 014502. [[CrossRef](#)]
26. Ghaderpour, E.; Pagiatakis, S.D. LSWAVE: A MATLAB software for the least-squares wavelet and cross-wavelet analyses. *GPS Solut.* **2019**, *23*, 50. [[CrossRef](#)]
27. Saeed, E.A.; Abdulhassan, K.M.; Al-Atbee, O.Y. Series and Parallel Arc Fault Detection in Electrical Buildings Based on Discrete Wavelet Theory. *Iraqi J. Electr. Electron. Eng.* **2021**, *17*, 94–101. [[CrossRef](#)]
28. Lu, W.; Gao, L.; Liu, Q.; Zhang, J.; Zhang, H. Electrode-width-weighted wavelet transform processor using SAW devices. *Microelectron. Int.* **2017**, *34*, 75–83. [[CrossRef](#)]
29. Wen, C.; Zhu, C.; Ju, Y.; Qiu, Y.; Xu, H.; Lu, W. Optimal frequency band design scheme of dyadic wavelet processor array using surface acoustic wave devices. *IEEE Trans. Ind. Electron.* **2008**, *56*, 949–955. [[CrossRef](#)]
30. Russell, B.; Han, J. Jean Morlet and the continuous wavelet transform. *CREWES Res. Rep.* **2016**, *28*, 115.
31. Lee, D.T.; Yamamoto, A. Wavelet analysis: Theory and applications. *Hewlett Packard J.* **1994**, *45*, 44. [[CrossRef](#)]
32. Büssov, R. An algorithm for the continuous Morlet wavelet transform. *Mech. Syst. Signal Process* **2007**, *21*, 2970–2979. [[CrossRef](#)]

33. Campbell, C. *Surface Acoustic Wave Devices and Their Signal Processing Applications*; Elsevier: Amsterdam, The Netherlands, 2012. [[CrossRef](#)]
34. Xu, H.; Jin, H.; Dong, S.; Song, X.; Chen, J.; Xuan, W.; Luo, J. Mode analysis of Pt/LGS surface acoustic wave devices. *Sensors* **2020**, *20*, 7111. [[CrossRef](#)]
35. Govindarajan, R.; Rojas-Nastrucci, E.; Kim, D. Surface Acoustic Wave-Based Flexible Piezocomposite Strain Sensor. *Crystals* **2021**, *11*, 1576. [[CrossRef](#)]
36. Liu, S.; Lu, W.; Zhu, C. Research on two-port network of wavelet transform processor using surface acoustic wavelet devices and its application. *Ultrasonics* **2017**, *81*, 81–85. [[CrossRef](#)] [[PubMed](#)]
37. Lu, W.; Zhu, C.; Kuang, L.; Zhang, T.; Zhang, J. Solution to the influence of the MSSW propagating velocity on the bandwidths of the single-scale wavelet-transform processor using MSSW device. *Ultrasonics* **2012**, *52*, 145–150. [[CrossRef](#)] [[PubMed](#)]
38. Mishra, D. Modeling of Interdigital Transducer Surface Acoustic Wave Device-Design and Simulation. In Proceedings of the 2015 Fifth International Conference on Communication Systems and Network Technologies, Gwalior, MP, India, 4–6 April 2015; pp. 1327–1331. [[CrossRef](#)]
39. Lu, W.; Zhu, C. Solving three key problems of wavelet transform processor using surface acoustic wave devices. *IEEE Trans. Ind. Electron.* **2010**, *57*, 3801–3806. [[CrossRef](#)]
40. Banupriya, R.; Venkatesan, T.; Pandiyarajan, G.; Pandya, H.M. SAW devices—A comprehensive review. *J. Environ. Nanotechnol.* **2014**, *3*, 106–115. [[CrossRef](#)]
41. Skeie, H.; Engan, H. Second-order effects in acoustic surface-wave filters: Design methods. *Radio Electron. Eng.* **1976**, *46*, 207–220. [[CrossRef](#)]
42. Lu, W.; Gao, L.; Zhang, J. A novel electrode-area-weighted method of implementing wavelet transform processor with surface acoustic wave device. *Int. J. Circuit Theory Appl.* **2016**, *44*, 2134–2146. [[CrossRef](#)]
43. Elsherbini, M.M.; Elkordy, M.F.; Gomaa, A.M. Design and Simulation for UHF oscillator using SAWR with different schematics. *Indones. J. Electr. Eng. Comput. Sci.* **2016**, *1*, 294–299. [[CrossRef](#)]
44. Elkordy, M.F.; Elsherbini, M.M.; Gomaa, A.M. Modeling and simulation of unapodized surface acoustic wave filter. *Afr. J. Eng. Res.* **2013**, *1*, 1–5.
45. Elsherbini, M.M.; Elkordy, M.F.; Gomaa, A.M. Towards a Simple Model for SAW Delayline Using CAD. *Am. J. Circuits Syst. Signal Process* **2015**, *1*, 86–92.
46. Elsherbini, M.M.; Elkordy, M.F.; Gomaa, A.M. Using COMSOL to model high frequency surface acoustic wave (SAW) device. *J. Electr. Electron. Eng. Res.* **2016**, *8*, 1–8. [[CrossRef](#)]
47. Gomaa, A.M.; Elkordy, M.F.; Elsherbini, M.M. A computer Simulation for The Response of an Apodized SAW Filter. *J. Electr. Eng.* **2014**, *14*, 6.
48. Elsherbini, M.M.; Elkordy, M.F.; Gomaa, A.M. Scattering Parameters prediction for 433MHz SAWR with Minimum Insertion loss. *Indones. J. Electr. Eng. Comput. Sci.* **2016**, *1*, 78–87. [[CrossRef](#)]
49. Elsherbini, M.M.; Elkordy, M.F.; Gomaa, A.M. Analytical modeling and simulation of SAW filter using concave. *Telkommika Indones. J. Electr. Eng.* **2015**, *16*, 495–501. [[CrossRef](#)]
50. Geng, W.; Zhao, C.; Xue, F.; Qiao, X.; He, J.; Xue, G.; Chou, X. Influence of Structural Parameters on Performance of SAW Resonators Based on 128° YX LiNbO<sub>3</sub> Single Crystal. *Nanomaterials* **2019**, *12*, 2109. [[CrossRef](#)]
51. Yang, B.; Lu, W.; Gao, L.; Feng, Y. Methods of Solving Passband Ripples and Sidelobes for Wavelet Transform Processor Using Surface Acoustic Wave Device. *IEEE Trans. Ind. Electron.* **2022**, *70*, 2897–2906. [[CrossRef](#)]